polarization. This transition is $^3B_2 \rightarrow {}^3B_2$, because of its b ($\vec{E} \| z$) polarization. This then reverses the order of the *middle two* transitions. The other two transitions are assigned as $^3B_2 \rightarrow {}^3A_2$, $^3B_1$.

The spin-allowed transitions in Ni(salmedpt) are $^3B_2 \rightarrow {}^3A_2$, $^3B_1$ (8600 cm^{-1}), $^3B_2$ (10,000 cm^{-1}), $^3A_2$, $^3B_1$ (13,960 cm^{-1}), and $^3A_2$, $^3B_1$ (17,300 cm^{-1}).

Spin-Forbidden Transitions in Ni(salmedpt). Two transitions which can be classified as spin forbidden occur at 11,800 and 13,300 cm^{-1}. The 11,800-cm^{-1} band also occurs in the spectrum of Ni(saldipa). The band at 13,300 cm^{-1} may be related to a band which lies under an allowed transition in Ni(saldipa). If the true electronic symmetry is C_{2v}, then transitions to singlet states should obey selection rules based on the double group C_2'. The correlation for $C_{2v} \rightarrow C_2'$ is given in Table V. The singlet transitions are $^3B_2 \rightarrow {}^1A_1$, $^1A_1 + {}^1B_2$, and $^1A_2 + {}^1B_1$. The direct product of the ground state and the first singlet excited state transforms as Γ_2. The direct product of the ground state and the second and third excited states transforms as $\Gamma_1 + \Gamma_2$. All allowed transitions will couple with these irreducible representations to produce transitions which are very weakly allowed parallel to either z or x,y. All transitions to singlet states are then very weakly allowed and the relative intensity of these transitions would be expected to be slightly stronger with $\vec{E} \| b$ than with $\vec{E} \| a$ since the allowed bands in the near-infrared region are stronger in b polarization.

Conclusion

The effective electronic symmetries about the Ni(saldipa) are different. Ni(saldipa) best fits D_{3h} symmetry and Ni(salmedpt) exhibits C_{2v} symmetry. This is surprising in view of the very similar geometry of the five atoms closely coordinated to nickel in both cases. However, the polarization data demand this type of interpretation. There are two possible interpretations for this difference in electronic symmetry. It is possible that either the differences in bond angles or the fact that N(1) is secondary in Ni(saldipa) and tertiary in Ni(salmedpt) could cause a difference in effective electronic symmetry. The angular differences are small: the largest is 5° for O(1)-Ni-O(2). The fact that transitions in Ni(saldipa) can be assigned on the basis of D_{3h} symmetry where the O(1)-Ni-O(2) angle is 25° larger than the ideal trigonal angle rules out the first possibility. Therefore we must conclude that the bonding about nitrogen strongly influences the effective electronic symmetry in these compounds.

Table V. Correlation Table for $C_{2v} \rightarrow C_2'$

C_{2v}	→	C_2	→	C_2'
A_1		A		Γ_1
A_2		A		Γ_1
B_1		B		Γ_2
B_2		B		Γ_2

Registry No. Ni(saldipa), 40685-46-9; Ni(salmedpt), 40754-29-8.

Acknowledgment. We wish to thank Professor Ciampolini for permission to reprint his crystal field diagrams and the National Science Foundation which supported this work in part through Grant GP 15432.

Contribution from Department of Chemistry,
North Carolina State University, Raleigh, North Carolina 27607

Magnetic Circular Dichroism, Crystal Field, and Related Studies of Nickel(II) Amines

A. F. SCHREINER* and D. J. HAMM

Received August 8, 1972

Complexes $[Ni(NH_3)_6]A_2$ ($A = ClO_4^-$, Cl^-), *trans*-$[Ni(py)_4L_2]Q$ ($L = NCO^-$, NCS^-, $NCSe^-$, N_3^-, py), and *trans*-$[Ni(py)_4X_2]$ ($X = Cl^-$, Br^-, I^-) have been examined by obtaining variously MCD, low-temperature electronic, and laser Raman data, crystal field parameters from the rapid Newton-Raphson solution-seeking method, and single-crystal X-ray data. New vibronic fine structure was observed and band assignments were made, and MCD parameters from moment analysis and gaussian decompositions were compared. Overall the MCD data can be understood by the recently proposed model of Harding, Mason, Robbins, and Thomson for $[Ni(NH_3)_6]^{2+}$. Finally, it was found that the single-crystal X-ray diffraction data for $[Ni(py)_4I_2]$ gave orthorhombic space group $D_{2h}{}^{14}$, $Z = 4$, and cell dimensions 9.678, 16.076, and 14.004 Å for a, b, and c. The planes of the pyridine rings were found to make an approximate angle of 45° with the (NiN_4) plane of the coordination sphere, similar to the *assumed* angle of the previously studied Cl^- and Br^- complexes. The two average nickel-ligand atom distances are 2.11 and 2.88 Å for Ni–N and Ni–I, respectively.

Introduction

Having the interest of characterizing properties of electronic excited states, we are particularly interested in determining what contributions the magnetic circular dichroism (MCD) technique can make toward achieving that goal. The method appeared especially suitable for the six-coordinate Ni(II) molecules of interest here (O_h and D_{4h}), since Faraday A parameters should in principle be extractable for orbital $T(O_h)$ and $E(D_{4h})$ states, and these parameters would also characterize such states[1] and in principle immediately distinguish them from nondegenerate orbital states. While the required interpretations turned out to be more complex,[2,3] the MCD data permitted several important new conclusions to be drawn. Thus the substance of this communication is based on the MCD information, 77°K electronic absorption spectra, crystal field calculations, and ir and laser Raman band locations in far-ir and lattice mode regions. Several X-ray parameters of a *trans*-$[Ni(py)_4I_2]$ crystal are also given.

There have also appeared a number of other interesting

(1) A. D. Buckingham and P. J. Stephens, *Annu. Rev. Phys. Chem.*, 17, 399 (1966).

(2) M. J. Harding, S. F. Mason, D. J. Robbins, and A. J. Thomson, *J. Chem. Soc. A*, 3047 (1971).

(3) M. J. Harding, S. F. Mason, D. J. Robbins, and A. J. Thomson, *J. Chem. Soc. A*, 3058 (1971).

papers on nickel(II)-pyridine compounds prior to this study. Most of these clarified electronic ground states[4-14] through vibrational analysis, etc., but electronic absorption studies have also been reported.[8-11,15-19] In fact, the recognition of orbital E(D_{4h}) states by means of crystal field theory[17] prompted us at the initial stage simply to measure the magnitudes of Faraday A parameters in order to extract excited-state orbital angular momenta. The recent MCD analysis of the intensities of $[Ni(H_2O)_6]^{2+}$ and $[Ni(NH_3)_6]^{2+}$ [2,3] mitigates against such a simple interpretation of octahedral Ni(II) compounds and their *apparent* Faraday parameters, however.

Experimental Section

1. Preparation of Compounds. All chemicals were reagent grade and used without further purification, except pyridine which was passed through a column of alumina in order to dry and decolorize it. Where necessary the pyridine was further dried over BaO and distilled from CaH_2.

The $Ni(NH_3)_6X_2$ complexes were prepared as described in the literature.[20a] The $[Ni(py)_4X_2]$ complexes (X^- = Cl^-, Br^-, NCO^-, NCS^-, $NCSe^-$) were also synthesized according to literature methods.[17,20b] During the preparation of the selenocyanate complex it was found that pyridine should always be added first to prevent the precipitation of selenium.[11] The iodo complex was synthesized according to the method of Nelson and Shepherd[10] from NiI_2 prepared *in situ*.[21] $[Ni(py)_4(N_3)_2]$ was prepared just prior to usage by dissolution of $Ni(py)_2(N_3)_2$ in warm, dry pyridine. Another method has also been published.[11] Large blue-green crystals readily formed upon cooling to warm temperature. $Ni(py)_2(N_3)_2$ itself was prepared by mixing an aqueous solution of hydrated nickel nitrate (1 mol) with an aqueous solution of sodium azide (2 mol) to which was added an aqueous solution of pyridine (*ca.* 2.5 mol). The light green, amorphous product, which formed immediately, analyzed properly for $Ni(py)_2(N_3)_2$. This complex is quite stable, is easily prepared, and is a good starting material for the less stable $[Ni(py)_4(N_3)_2]$ complex.

Nickel analyses were performed in this laboratory by means of EDTA titration using murexide as the indicator.[22] Carbon, nitrogen, and hydrogen analyses were carried out by Galbraith Laboratories, Inc., Knoxville, Tenn. 37921.

Nitrogen in the hexaammine complexes was analyzed in this laboratory *in situ* by means of the Winkler modification of the Kjeldahl titration for free ammonia. Brom Cresol Green was used as the indicator.[23] The percentage compositions follow. *Anal.* Calcd for $Ni(NH_3)_6Cl_2$: Ni, 25.33; N, 36.24. Found: Ni, 25.14; N, 36.0. Calcd for $Ni(NH_3)_6(ClO_4)_2$: Ni, 16.3; N, 23.34. Found: Ni, 16.3; N, 23.1. Calcd for $[Ni(C_5H_5N)_4Cl_2]$: Ni, 13.16; C, 53.95; N, 12.03; H, 4.57. Found: Ni, 12.82; C, 52.21; N, 12.15; H, 4.22. Calcd for $[Ni(C_5H_5N)_4Br_2]$: Ni, 10.98; C, 44.96; N, 10.50; H, 3.78. Found: Ni, 10.97; C, 43.74; N, 9.90; H, 3.70. Calcd for $[Ni(C_5H_5N)_4I_2]$: Ni, 9.34; C, 38.18; N, 8.94; H, 3.32. Found: Ni, 9.27; C, 38.29; N, 9.11; H, 3.32. Calcd for $[Ni(C_5H_5N)_4(NCO)_2]$: Ni, 12.79; C, 57.55; N, 18.30; H, 4.39. Found: Ni, 12.82; C, 58.00; N, 18.23; H, 4.41. Calcd for $[Ni(C_5H_5N)_4(NCS)_2]$: Ni, 11.95; C, 53.78; N, 17.11; H, 4.10. Found: Ni, 11.99; C, 54.24; N, 17.04; H, 4.16. Calcd for $[Ni(C_5H_5N)_4(NCSe)_2]$: Ni, 10.03; C, 45.15; N, 14.36; H, 3.45. Found: Ni, 10.07; C, 45.16; N, 14.49; H, 3.29. $[Ni(py)_4(N_3)_2]$ was prepared *in situ* just before the experiment by adding $Ni(py)_2(N_3)_2$ to dry pyridine.

2. Instrumentation. Near-ir data were obtained on a Perkin-Elmer 521 spectrometer (polystyrene calibration), far-ir spectra were recorded on a Perkin-Elmer FIS-3 instrument (H_2O vapor calibration), and the Raman bands were located using a Jarrell-Ash 25-300 spectrometer and the 4880-Å Ar line of a 52G argon–krypton laser (Coherent Radiation). Electronic absorption spectra of solutions and mulls were obtained with a Cary 14 spectrophotometer. Samples were cooled in a quartz exchange-gas (He) dewar, and the temperature was carefully monitored with a copper–constantan thermocouple contacting the sample, with the output voltage being read on a Leeds–Northrup Type K-3 Universal potentiometer and Leeds–Northrup 2430-C galvanometer.

MCD measurements were carried out as described elsewhere.[24] When electronic spectra are shown with MCD spectra, then both were obtained on the JASCO instrument. Through careful calibration it was found that the less accurate JASCO wavelength reading (λ_J) relate to correct values (λ_c) through $\lambda_c = 1.018\lambda_J - 6.003 \times 10^{-5}\lambda_J^2$. MCD parameters of Tables V-VII were derived after conversion to λ_c, and dipole strengths from Cary 14 data.

Solutions for spectral measurements were prepared by dissolving compounds in pyridine–chloroform (1:9 v/v) solvent with the exception of the diazido complex, which was obtained by dissolving a known quantity of $Ni(py)_2(N_3)_2$ in dry pyridine. Mulls of $[Ni(py)_4(N_3)_2]\cdot 2py$ in Kel-F gave reproducible spectra when they were obtained soon after preparation. The mull spectrum of $[Ni(py)_4(NCSe)_2]$ was not obtained because the complex decomposed in the mulling process in Kel-F, Fluorolube, and Nujol. While the visible portion of the spectra were obtained very near liquid N_2 temperature (see spectra), the spectra of the near-ir region ($\lambda \geq 700$ nm) were recorded at *ca.* 100°K due to the nature of the Cary construction. However, the temperatures of all spectra shown here are equilibrium temperatures.

Results and Discussion

In this section we will deal with new electronic absorption information and assignments of the important hexaammine, $[Ni(NH_3)_6]^{2+}$, and a brief discussion of the relevant, recent MCD interpretation of this moiety will be presented, since it leads directly to the understanding of the MCD of the analogous hexapyridine complex, $[Ni(py)_6]^{2+}$, and to the MCD data of the series of pseudohalogen substitution molecules, *trans*-$[Ni(py)_4L_2]$ (L^- = NCO^-, NCS^-, $NCSe^-$, N_3^-). The new 80°K electronic absorption data of *trans*-$[Ni(py)_4I_2]$ will also be detailed, and its bonding parameters and band assignments will be compared with those of the previously studied *trans*-$[Ni(py)_4X_2]$ (X^- = Cl^-, Br^-). The MCD data of *trans*-$[Ni(py)_4X_2]$ (X^- = Cl^-, Br^-, I^-) will be discussed, and several details of our single-crystal X-ray structural study of $[Ni(py)_4I_2]$ will also be given.

1. Electronic Absorption Spectra of $[Ni(NH_3)_6]X_2$ (X^- = ClO_4^-, Cl^-) at Liquid Nitrogen Temperature. The low-temperature mull electronic absorption spectrum of the d-d transitions of $[Ni(NH_3)_6](ClO_4)_2$ between 1200 and 300 nm is shown in Figure 1. The temperatures of the visible and near-ir portions of this spectrum were recorded at 80 and 100°K, respectively. Figure 2 shows in greater detail the partial spectrum (80°K) of the transition to $^3T_{1g}(t_2^5e^3)$ and to the intraconfigurational $^1A_{1g}(t_2^6e^2)$ excited state. These are the most detailed, structural spectra yet obtained, although ambient-temperature solution spectra of the [Ni-

(4) N. S. Gill, R. H. Nuttal, D. E. Scaife, and D. W. A. Sharp, *J. Inorg. Nucl. Chem.*, **18**, 79 (1961).
(5) R. J. H. Clark and C. S. Williams, *Inorg. Chem.*, **4**, 350 (1965).
(6) R. J. H. Clark and C. S. Williams, *Spectrochim. Acta*, **22**, 1081 (1966).
(7) R. H. Nuttal, A. F. Cameron, and D. W. Taylor, *J. Chem. Soc. A*, 3103 (1971).
(8) W. E. Bull and L. E. Moore, *J. Inorg. Nucl. Chem.*, **27**, 1341 (1965).
(9) H. G. Mayfield, Jr., and W. E. Bull, *Inorg. Chim. Acta*, **3**, 676 (1969).
(10) S. M. Nelson and T. M. Shepherd, *J. Chem. Soc.*, 3276 (1965).
(11) S. M. Nelson and T. M. Shepherd, *Inorg. Chem.*, **4**, 813 (1965).
(12) J. A. Happe and R. L. Ward, *J. Chem. Phys.*, **39**, 1211 (1963).
(13) R. E. Cramer and R. S. Drago, *J. Amer. Chem. Soc.*, **92**, 66 (1970).
(14) D. Forster, *Inorg. Chim. Acta*, **5**, 465 (1971).
(15) M. R. Rosenthal and R. S. Drago, *Inorg. Chem.*, **4**, 840 (1965).
(16) O. Bostrup and C. K. Jorgensen, *Acta Chem. Scand.*, **11**, 1223 (1957).
(17) D. A. Rowley and R. S. Drago, *Inorg. Chem.*, **6**, 1092 (1967).
(18) D. A. Rowley and R. S. Drago, *Inorg. Chem.*, **7**, 795 (1968).
(19) J. Reedijk, P. W. N. M van Leewwen, and W. L. Groenveld, *Recl. Trav. Chim. Pays-Bas*, **87**, 129 (1968).
(20) (a) G. G. Schlessinger, "Inorganic Laboratory Preparations," Chemical Publishing Co., New York, N. Y., 1962, p 194; (b) G. B. Hauffman, R. A. Albers, and F. L. Harlan, *Inorg. Syn.*, **12**, 251 (1971).
(21) D. M. L. Goodgame and L. M. Vananzi, *J. Chem. Soc.*, 616 (1963).
(22) H. A. Flaschka, "EDTA Titrations; an Introduction to Theory and Practice," Pergamon Press, New York, N. Y., 1959, p 79.
(23) W. C. Pierce, E. L. Haenisch, and D. T. Sawyer, "Quantitative Analysis," 4th ed, Wiley, New York, N. Y., 1958, p 260.
(24) A. F. Schreiner and P. J. Hauser, *Inorg. Chem.*, **11**, 2706 (1972).

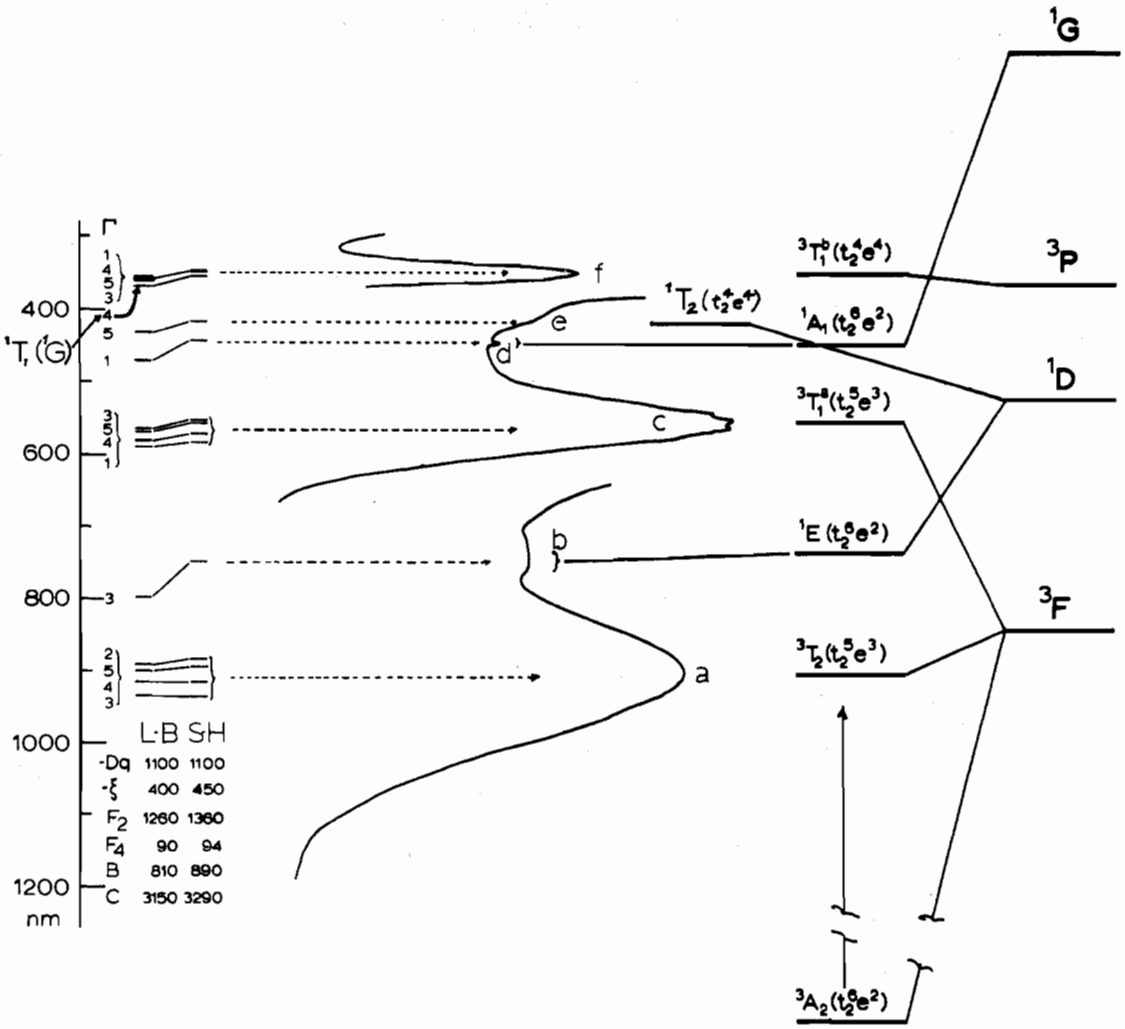

Figure 1. Liquid N_2 spectrum of $[Ni(NH_3)_6](ClO_4)_2$ in a Kel-F mull. Band locations of Liehr and Ballhausen[26] (L-B) and of this study (S-H) using crystal field theory are shown on the far left of the figure.

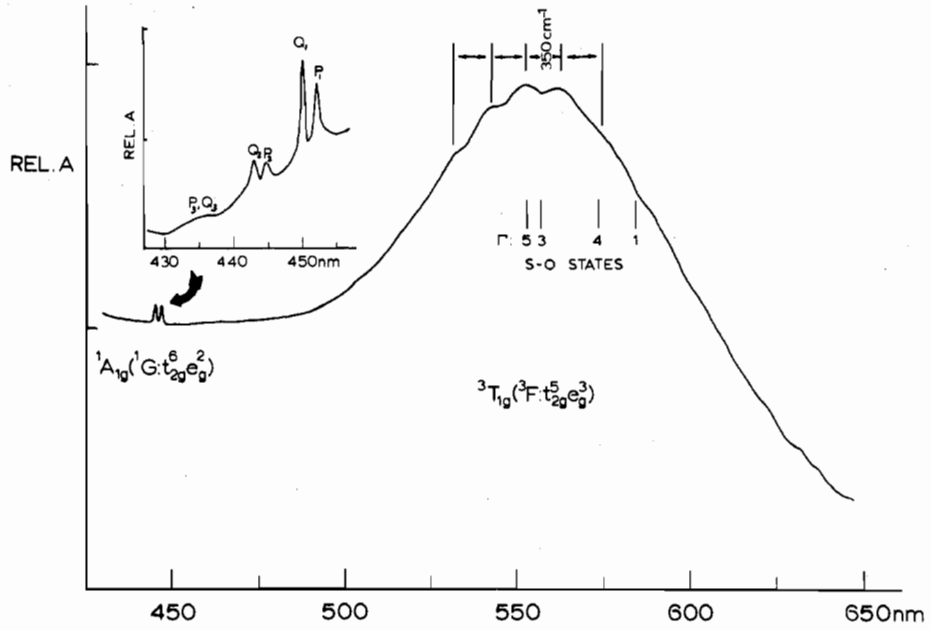

Figure 2. $^3T_{1g}(F)$ and $^1A_{1g}(G)$ bands of $[Ni(NH_3)_6](ClO_4)_2$ at 80°K. The insert of $^1A_{1g}$ is for $[Ni(NH_3)_6]Cl_2$.

$(NH_3)_6]^{2+}$ cation have appeared in several places.[19,25] The left-hand side of Figure 1 labels the states which Liehr and Ballhausen[26] assigned to bands a, b, c, and f of the solution spectrum, in agreement with earlier conclusions. Most states,

(25) (a) C. K. Jorgensen, *Acta Chem. Scand.*, 9, 1362 (1955); (b) O. G. Holmes and D. S. McClure, *J. Chem. Phys.*, 26, 1686 (1957).

(26) A. D. Liehr and C. J. Ballhausen, *Mol. Phys.*, 2, 123 (1959).

such as the ones labeled in Figure 1, were also found for the related $[Ni(en)_3](NO_3)_2$ by Karipides[27a] and Dingle and Palmer.[27b]

Our new observations for the hexaammine complex include (1) the five-component fine structure on $^3T_{1g}(t_2^5e^3)$ (band c; see Figures 1 and 2), (2) the multicomponent fine structure of $^1A_{1g}(t_2^6e^2)$ (band d; Figures 1 and 2), and (3) uncovering of band e which is assigned to $^1T_{2g}(t_2^4e^4)$. Since Ni^{2+} has a rather large one-electron spin-orbit coupling constant ($\zeta = 630$ cm^{-1}),[28] we used the "complete" theory of Liehr and Ballhausen to investigate the crystal field parameters that best account for our low-temperature spectrum. Using their d^2 matrices[29] the latter authors found the following parameters adequate for the solution spectrum: $-Dq = 1100$ cm^{-1}, $-\zeta = 400$ cm^{-1}, $B = 810$ cm^{-1}, and $C = 3150$ cm^{-1} (or $F_2 = 14F_4$). These parameters, however, underestimated the positions of spin-forbidden bands which were located at 80°K, *i.e.*, $^1E_g(D)$, $^1T_{2g}(D)$, and $^1A_{1g}(G)$. For this reason we deviated from the rule $F_2 = 14F_4$ and found that the higher value $B = 890$ cm^{-1} and $C = 3290$ cm^{-1} were more suitable. Calculated and experimental band locations are given in Table I.

We now turn our attention to the band structures of $^3T_{1g}(t_2^5e^3)$ and to the intraconfigurational transition $^3A_{2g}$-$(t_2^6e^2) \rightarrow {}^1A_{1g}(t_2^6e^2)$ as shown in Figure 2. We first consider the fine structure associated with the more intense spin-allowed $^3T_{1g}$ band. Thus, using the "complete" theory of Liehr and Ballhausen, wherein first- and second-order spin-orbit coupling was included, we found it impossible to separate the Γ_1, Γ_3, Γ_4, and Γ_5 components of $^3T_{1g}$ by equal amounts as observed at 80°K. Computationally, Γ_3 and Γ_5 remain close to each other so that only *three* spin-orbit components are predicted to be distinct. However, we can identify five about equally spaced components on this band so that we rule them out as spin-orbit structure and assign them as members of dominating vibronic progression having average spacing of 330 ± 20 cm^{-1}. This corresponds closely to the a_{1g} skeletal fundamental of (NiN_6) which we were able to observe at 362 cm^{-1} in the Raman spectrum.[30] Since only t_{1u} or t_{2u} vibrations, Γ_μ, can make $^3A_{2g} \rightarrow {}^3T_{1g}$ allowed, one concludes therefore that the observed vibronic progression may correspond to excitations to advanced members of $|^3T_{1g} \cdot \Gamma_\mu \cdot n a_{1g}\rangle$; *i.e.*, $(\Gamma_\mu \cdot n a_{1g})$ are combination levels, coupled to $^3T_{1g}$, of the fundamental Γ_μ and overtones of the a_{1g} mode. Similar excitation processes have been observed by others (ref 2 and citations therein). We have found a similar progression upon $^3T_{1g}$ of the analogous $[Ni(NH_3)_6]Cl_2$. Our 4°K work under way on this $[Ni(NH_2)_6]X_2$ series is expected to identify Γ_μ on the red side of $^3T_{1g}$. Indeed it may become apparent that the $^3T_{1g}$ progression is uniquantal in t_{1u}^{ν} of ~330 cm^{-1}.[31]

The discovery of a doublet for the intraconfigurational $(t_2^6e^2)$ transition $^3A_{2g} \rightarrow {}^1A_{1g}(G)$ (band d of Figure 1), located at about 450 nm, led us to reinvestigate this region also more closely. We were thus able to find additional fine structure for this transition in a number of $[Ni(NH_3)_6]A_2$ complexes. This $^1A_{1g}$ region is shown in Figure 2 (insert)

(27) (a) A. G. Karipidis, Ph.D. Dissertation, University of Illinois, 1964; (b) R. Dingle and R. A. Palmer, *Theor. Chim. Acta*, **6**, 249 (1966).

(28) B. N. Figgis, "Introduction to Ligand Fields," Interscience, New York, N. Y., 1966, p 60.

(29) A. D. Liehr and C. J. Ballhausen, *Ann. Phys. (New York)*, **6**, 134 (1959).

(30) A full report on the laser Raman results of $[Ni(NH_3)_6]^{2+}$ will be forthcoming.

(31) J. M. Terrasse, H. Poulet, and J. P. Mathieu, *Spectrochim. Acta*, **20**, 305 (1964).

Table I. Computed and Experimental (80°K) Energies of d-d Transitions in $[Ni(NH_3)_6](ClO_4)_2$

Assignment[a]			Band locations, cm^{-1}	
State	Origin	SOC[b]	Calcd	Exptl
$^3T_{2g}$	F: $t_2^5e^3$	Γ_3	10,761	11,050 (905 nm)
		Γ_4	10,900	
		Γ_5	11,152	
		Γ_2	11,269	
^1E_g	D: $t_2^6e^2$	Γ_3	13,355	13,333
$^3T_{1g}$	F: $t_2^5e^3$	Γ_1	17,148	18,018 (555 nm)
		Γ_4	17,457	
		Γ_5	17,917	
		Γ_3	18,013	
$^1A_{1g}$	G: $t_2^6e^2$	Γ_1	22,658	22,450 (445.5 nm)
$^1T_{2g}$	D: $t_2^4e^4$	Γ_5	23,905	24,242 (412.5 nm)
$^1T_{1g}$	G: $t_2^5e^3$	Γ_4	28,281	*c*
$^3T_{1g}$	P: $t_2^4e^4$	Γ_3	28,667	28,570 (350.0 nm)
		Γ_5	28,749	
		Γ_4	28,922	
		Γ_1	28,980	

18,750, 18,416, 18,083, 17,746, 17,410

[a] Ground state is $^3A_{2g}(t_2^6e^2)$. [b] The equivalent Mulliken notation for the spin-orbit components is $\bar{A}_1$, $\bar{A}_2$, $\bar{E}$, $\bar{T}_1$, and $\bar{T}_2$ for Γ_1, Γ_2, Γ_3, Γ_4, and Γ_5, respectively. [c] Not discernible.

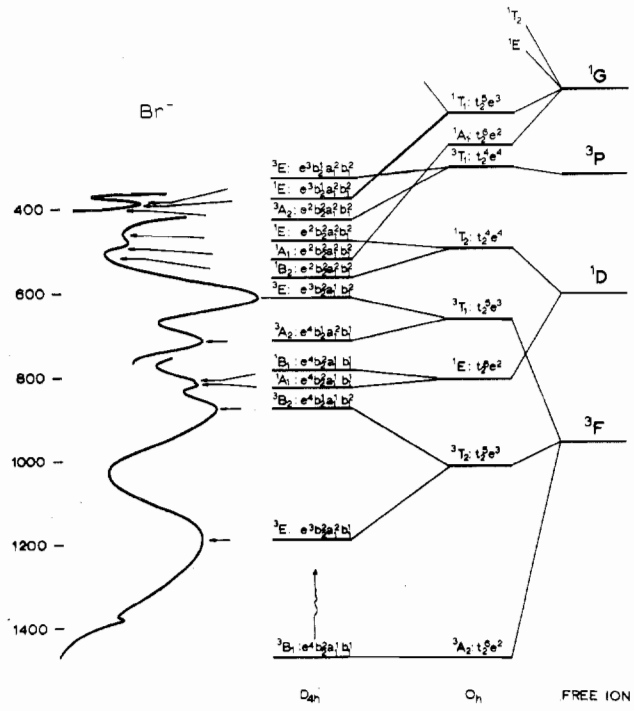

Figure 3. Liquid N_2 spectrum of $[Ni(py)_4Br_2]$ in Kel-F and predicted states (ref 17 and this work).

for $A^- = Cl^-$, for example. We identified first members of each of two progressions, *P* and *Q*. Thus, we have differences $Q_2 - Q_1 = P_2 - P_1 = 360 \pm 10$ cm^{-1}, and this corresponds nicely to the intense a_{1g} skeletal (NiN_6) modes[30] of our Raman spectra (370 cm^{-1} for Cl^- and 362 cm^{-1} for ClO_4^-). Since the electronic transition involves no population change in orbitals pointing to ligands, one expects, as indeed we found, the above agreement between vibrational frequencies and progression spacings. This supports our assignment of spacings in *P* and *Q*. The second interesting feature of the $^3A_{2g} \rightarrow {}^1A_{1g}$ transition is the 105 ± 10 cm^{-1} lag of the *Q* progression behind the *P* progression, *i.e.*, $Q_1 - P_1 \approx Q_2 - P_2 \cong 105 \pm 10$ cm^{-1}. This corresponds most closely to the difference between the t_{1u} skeletal (NiN_6) bending fundamental, t_{1u}^a, at 215 cm^{-1} and the t_{1u} skeletal stretching fundamental, or t_{1u}^b, at 334 cm^{-1}.[31] Thus, the selection rules for the combined effects of vibronic coupling and spin-orbit coupling lead to the assignment

$\bar{T}_2(^3A_{2g}) \rightarrow \bar{A}_1(^1A_{1g})$, or $0 \rightarrow 0$	Forbidden (and missing)
$\rightarrow \bar{A}_1(^1A_{1g}) + t_{1u}{}^a$	P_1
$\rightarrow \bar{A}_1(^1A_{1g}) + t_{2u}{}^b$	Q_1
$\rightarrow \bar{A}_1(^1A_{1g}) + t_{1u}{}^a + a_{1g}$	P_2
$\rightarrow \bar{A}_1(^1A_{1g}) + t_{1u}{}^b + a_{1g}$	Q_2
$\rightarrow \bar{A}_1(^1A_{1g}) + t_{1u}{}^a + 2a_{1g}$	P_3, Q_3
$\rightarrow A_1(^1A_{1g}) + t_{1u}{}^b + 2a_{1g}$	P_3, Q_3

where $\bar{\Gamma}$ are the spin-orbit states. Thus, while t_{2u} could have been an allowing mode in principle, in fact only the t_{1u} modes help $^3A_{2g} \rightarrow {}^1A_{1g}$ obtain intensity. Finally, the decrease in intensity of each progression in the direction of higher energy is entirely consistent with our assignment of the details for this intraconfigurational transition.

2. **77°K Data and Crystal Field Parameters of *trans*-$[Ni(py)_4I_2]$.** Having first discussed data and crystal field results of the cubically coordinated Ni(II) of $[Ni(NH_3)_6](ClO_4)_2$ on the one hand, we discuss next the new electronic absorption spectrum at 77 and 103°K of the most severe tetragonally distorted Ni(II) complex of this series studied, $[Ni(py)_4I_2]$. It is also of interest to compare several of its crystal field parameters with those of the dichloro and dibromo analogs,[17,32] $[Ni(py)_4Cl_2]$ and $[Ni(py)_4Br_2]$ of earlier studies. We show first the previously assigned 77°K electronic absorption spectrum of $[Ni(py)_4Br_2]$ in Figure 3, and along with it we designated the excited-state labels of the tetragonal crystal field calculation of Rowley and Drago.[17] All the band maxima locations of this work can be found in Table II. Our data are sufficiently accurate to let us conclude that the transitions to spin triplets are vibronically allowed at least in part.

Turning our attention to the spectra (Figure 4) of $[Ni(py)_4I_2]$, it is immediately evident that tetragonal splittings Δt_1 and Δt_2 of $^3T_2(t_2{}^5e^3)$ and $^3T_1(t_2{}^5e^3)$, respectively, are significantly larger than for these same states of $[Ni(py)_4Br_2]$. The computed splittings of $^3T_1(P)$ are nearly the same, however.

	$[Ni(py)_4Br_2]$	$[Ni(py)_4I_2]$
Δt_1	3060 cm^{-1}	3930 cm^{-1}
Δt_2	2310 cm^{-1}	3235 cm^{-1}
$\Delta t_3[^3T_1(P)]$ (calcd)	1070 cm^{-1}	1190 cm^{-1}

The basis of our excited-state ordering for $[Ni(py)_4I_2]$ between ~1500 and ~500 nm requires some comments. We assumed that the sign of the crystal field parameter $Dt = {}^4/_7[Dq(py) - Dq(I^-)]$ must be positive in order for it to remain physically reasonable. First-order crystal field theory[32b] in the absence of state interaction then dictates that (1) $^3B_{2g} > {}^3E_g{}^a$ for $^3T_2$, since $E(^3B_{2g}) = 10Dq(py)$ and $E(^3E_g{}^a; T_2) = 10Dq(py) - {}^{35}/_4Dt$, and (2) $^3A_{2g} < {}^3E_g{}^b$ for $^3T_1(F)$, since $E(^3A_{2g}) = 10Dq(py) - 5Dt - 4Ds + 12B$ and $E(^3E_g{}^b; T_1, F) = 10Dq(py) - {}^{25}/_4Dt + 2Ds + 2B$, with the difference being $^3E_g{}^b - {}^3A_{2g} = -{}^5/_4Dt + 6Ds$ and $Dt < Ds > 0$ (see Table III). The dilemma which we initially encountered in assigning bands of $[Ni(py)_4I_2]$ was that of deciding which of bands b or c (Figure 4) to associate with $^3B_{2g}$ and which with $^1E_g{}^a$ in the region of 900 nm. The location of $^3B_{2g}$ should be invariant as X is varied in $[Ni(py)_4X_2]$, since even with complete matrices its energy is always $10Dq(py)$. However, this expectation is only an idealized one as evident from the data of $X^- = Cl^-$, Br^-, or I^- which are summarized in Table II. The use of Lever's[32b] tetragonal strong-field matrix elements for spin triplets permitted us to conclude that band c at 11,834 cm^{-1} must be the $^3B_{1g} \rightarrow {}^3B_{2g}(T_2)$ transition (Table II), and the crystal field parameters of our assignment are in column "A" of Table III. We reject the choice of band b as $^3B_{2g}$ because (1) the resulting parameters are unreasonably out of line (see column "B" of Table III) in this Cl, Br, I series and (2) the calculated energies of tetragonal components of $^3T_1(P)$, $^3A_{2g}$, and ^3E_g, are much too high by about 2500 cm^{-1} compared to the analogous compound $[Ni(py)_4Br_2]$; *viz.*, $^3A_{2g}$ is at 26,500 cm^{-1} and ^3E_g at 28,370 cm^{-1}. All these data then permit the comparison of several features of this interesting tetragonal series. The rapid method of extraction of the crystal field parameters was carried out by means of the variable-secant analog of the Newton-Raphson method.[33]

The following comparative conclusions are interesting up to this point. First, the ratio of $^3T_2$ tetragonal splittings is $\Delta t_1(Cl):\Delta t_2(Br):\Delta t_1(I) = 1.0:1.14:1.46$; the ratio of the $^3T_1(F)$ splittings is $\Delta t_2(Cl):\Delta t_2(Br):\Delta t_3(I) = 1.0:1.25:1.70$; and the ratio of $^3T_1(P)$ splittings is $\Delta t_3(Cl):\Delta t_3(Br):\Delta t_3(I) = 1.0:1.21:1.35$. Thus, the magnitude of splitting of these three orbital triplets is $Cl^- < Br^- < I^-$. The relative splittings of $^3T_2$ can easily be understood on physical grounds from first-order theory, since $\Delta t_1 = {}^{35}/_7[Dq(py) - Dq(X^-)]$ and $Dq(Cl^-) > Dq(Br^-) > Dq(I^-)$. The dominating term in the splitting of $^3T_1(F)$ with $^3E_g > {}^3A_{2g}$, on the other hand, is $6Ds$, or $\Delta t_2 = 6Ds - {}^5/_4Dt$, because $6Ds \gg {}^5/_4Dt$. With

$$Ds = \frac{2}{7}\left\{eQ(xy)\left[\frac{\langle r^2{}_{xy}\rangle}{R^3{}_{xy}}\right] - eQ(z)\left[\frac{\langle r^2{}_z\rangle}{R^3{}_z}\right]\right\}$$

and finding $Ds(I^-) > Ds(Br^-) > Ds(Cl^-)$, one can conclude that the trend in variation of the parameter $\langle r^2\rangle/R^3$ for the halogen ligands is $I^- < Br^- < Cl^-$. This result is of course expected to arise if the Ni(II)-X internuclear parameter R^3 increases more rapidly than the Ni(II) radial expectation value $\langle r^2\rangle$ in going from Cl^- to I^-, as is reasonable. The trend in the computed splitting of $^3T_1(P)$ is more difficult to analyze, since there is a more delicate balance between the two terms in $\Delta t_3 = 5Dt - 3Ds$, and off-diagonal state interaction elements can also play too large a role. The second conclusion is that the order of magnitudes of the splittings is $^3T_2 > {}^3T_1(F) > {}^3T_1(P)$ for each of the three compounds. Third, there are indeed variations in $Dq(py)$ as can be concluded from the experimental location of $^3B_{2g}$ in the three compounds. Fourth, the Racah B parameter of the iodo complex is about 60 cm^{-1} less than those of the chloro and bromo values. This is then reflected in the nephelauxetic ratio, β (Table III). Fifth, the variation of the absolute values of σ- and π-bonding interaction parameters, $|d\sigma|$ and $|d\pi|$, respectively, defined by McClure[34] as

$$d\sigma = (-)^{15}/_8(4Ds + Dt)$$

$$d\pi = (-)^5/_2({}^3/_5Ds - Dt)$$

is in the same order for these compounds: $Cl^- < Br^- < I^-$. Thus, this can be construed to mean that (1) the σ and π interactions of py with nickel are larger than those of the halide ions and (2) the difference between py and the halide ion increases in the order of $|d\sigma|$ and $|d\pi|$, or (py-Cl) < (py-Br) < (py-I), which means that, of the three halide ions, Cl is most like py.

Finally, there is a notable presence of first and second pyridine ν(C-H) overtones in the region of $^3T_2(t_2{}^5e^3)$ in

(32) (a) A. B. P. Lever, *Coord. Chem. Rev.*, 3, 119 (1968). Whereas these matrices are incomplete (this also led Mayfield and Bull[9] into error), the appropriate ones are given in ref 32b. (b) A. B. P. Lever, "Inorganic Electronic Spectroscopy," American Elsevier, New York, N. Y., 1968, p 409.

(33) C. E. Froberg, "Introduction to Numerical Analysis," Addison-Wesley, Reading, Mass., 1965, pp 15-42.

(34) D. S. McClure in "Advances in the Chemistry of Coordination Compounds," S. Kirshner, Ed., Macmillan, New York, N. Y., 1961, p 498.

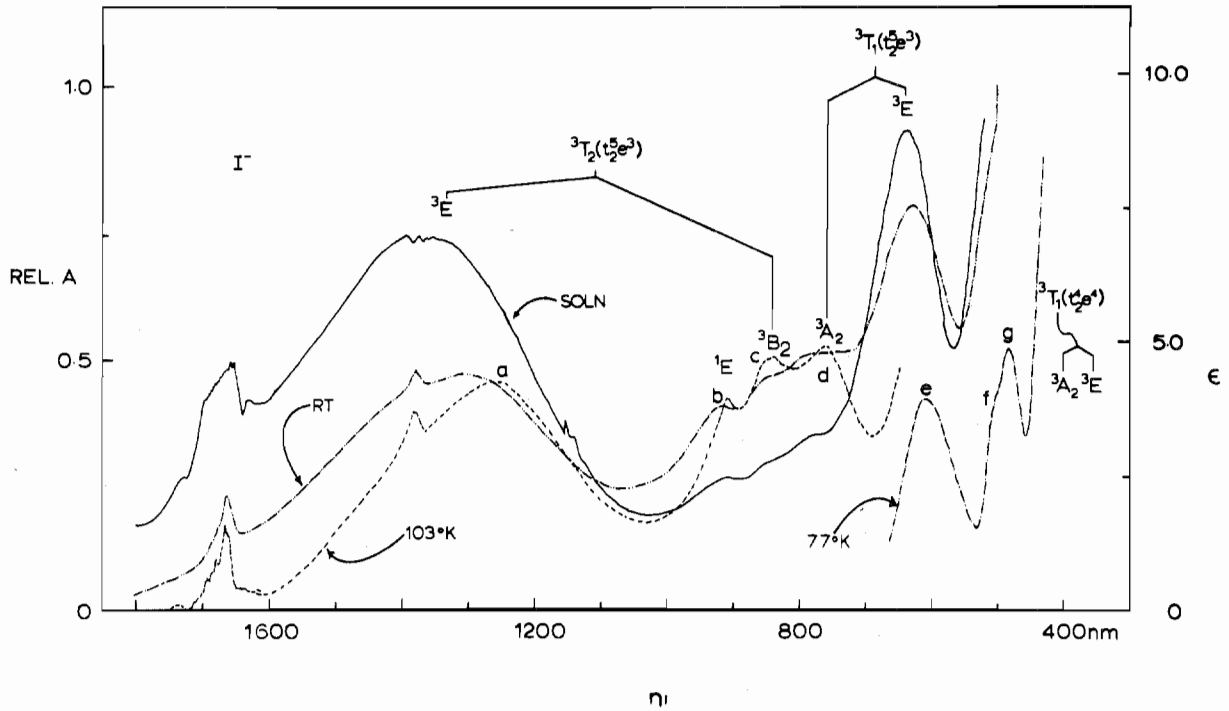

Figure 4. Spectra of $[Ni(py)_4I_2]$ under four conditions: solution, solid line; ambient Kel-F mull, dash-dot-dot; 103°K mull, dash; 77°K, dash-dot. Axis label ϵ is only for solution.

Table II. $^3B_{1g} \rightarrow {}^3T_{ng}$ Transition Energies (cm^{-1}) in *trans*-$[Ni(py)_4X_2]$

		$^3T_{2g}(F)$		$^3T_{1g}(F)$		$^3T_{1g}(P)$	
X^-		E_g[a]	B_{2g}	A_{2g}[a]	E_g[b]	A_{2g}[b]	E_g[c]
Cl^-	Obsd	9042 (1106 nm)	11,730 (853 nm)	14,930 (670 nm)	16,818 (595 nm)	?	26,759 (374 nm)
	Calcd	9042	11,730	14,931	16,819	25,607	26,489
	Δt	2688		1,888		882	
Br^-	Obsd	8430 (1186 nm)	11,490 (870 nm)	14,080 (710 nm)	16,390 (610 nm)	?	26,030 (384 nm)
	Calcd	8430	11,490	14,080	16,390	24,896	25,965
	Δt	3060		2,310		1,069	
I^-	Obsd	7905 (1265 nm)	11,834 (845 nm)	13,158 (760 nm)	16,393 (610 nm)	?	?
	Calcd (A)	7905	11,834	13,159	16,393	23,977	25,164
	Calcd (B)	7905	10,989	13,155	16,392	26,502	28,371
	Δt	3929		3,235		1,187	

Table III. Crystal Field Parameters (cm^{-1}) for *trans*-$[Ni(py)_4X_2]$ with Configuration Interaction

	X			
			I	
	Cl	Br	A	B
$Dq(xy)$	1173	1149	1183	1098
$Dq(z)$	680	598	496	596
Ds	496	631	819	1159
Dt	282	315	393	290
B	799	804	742	987
$\beta = B/B_0$	0.73	0.74	0.69	0.91
$d\pi$	−40	−159	−246	−1011
$d\sigma$	−1274	−1536	−1966	−2281

these dihalogen complexes; *viz.*, the dichloro compound has a band at ∼1120 nm, the dibromo compound also has one at 1120 nm, but the diiodo complex has, in addition to the ∼1120-nm band, an intense major band near 1680 nm (Figure 4). These two bands are clearly present in pyridine dissolved in CCl_4 (our 1400-nm band was an instrumental difficulty). These bands of the iodo complex became especially well defined at 103°K and in fact the spectra at temperatures of 114 and 117°K are necessary in order to see this structure in the chloro and bromo (Figure 3) analogs, respectively. The uncovering of the 1680-nm overtone of $[Ni(py)_4I_2]$ is especially dramatic, since the red half of $^3E(T_2)$ decreases significantly on cooling. Several overtones were also reported in ref 15.

3. 77°K Electronic Absorption Spectra of Pseudohalogen Derivatives. The d-d electronic absorption spectra of two dipseudohalogen compounds, $[Ni(py)_4L_2]$, recorded at various temperatures are shown in Figures 5 and 6 ($L^- = NCO^-$ and N_3^-). The spectra of $[Ni(py)_4(NCS)_2]$ are very similar to that for $L^- = NCO^-$ (Figure 5). The selenocyanato analog, $[Ni(py)_4(NCSe)_2]$, decomposed during sample preparation (grinding) for spectral measurements in Kel-F as well as in Nujol and Fluorolube, so that we can make reference only to its solution spectrum.[11] A summary of data can be found in Table IV.

An interesting feature about the low-temperature spectra of these pseudohalogen compounds is the occurrence of a red shoulder on the major intensity of $^3T_{1g}(t_2^5e^3)$ near 650 nm and near 700 nm for $[Ni(py)_4(NCO)_2]$ and $[Ni(py)_4(N_3)]$, respectively. The estimated separation of more than 2000 cm^{-1} from the relatively large $^3T_{1g}$ band maximum of each complex at about 600 nm rules them out as tetragonal components of $^3T_1$. The basis for this reasoning is the observation by Hare and Ballhausen[35] that the $^3T_{1g}$ components are separated by only 150 cm^{-1} in *trans*-$[Ni(NH_3)_4(NCS)_2]$, and furthermore, py and NCS^- ligands are even closer in the spectrochemical series than the NH_3-NCS pair. This con-

(35) C. R. Hare and C. J. Ballhausen, *J. Chem. Phys.*, **40**, 792 (1964).

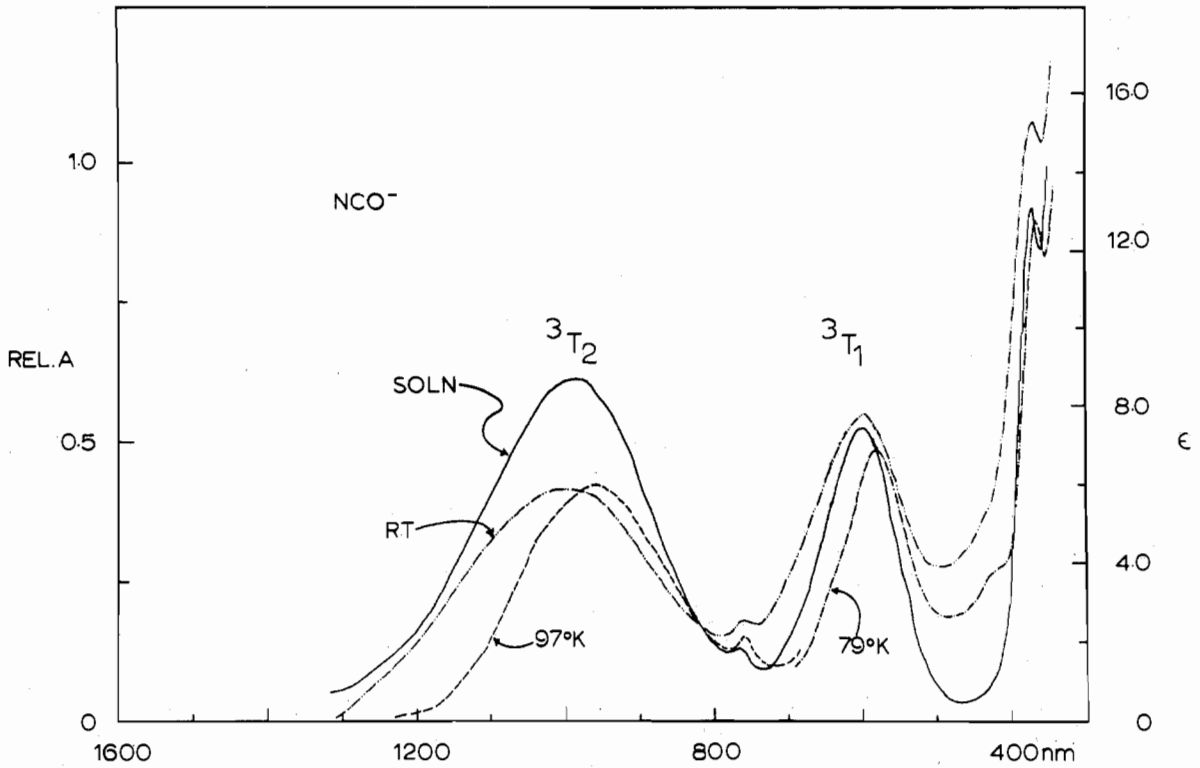

Figure 5. Electronic spectra of $[Ni(py)_4(NCO)_2]$ under these conditions: solution, solid line; Kel-F mull at ambient temperature, dash-dot-dot; 97°K, dash; 79°K, dash-dot. The axis of label ϵ applies to the solution.

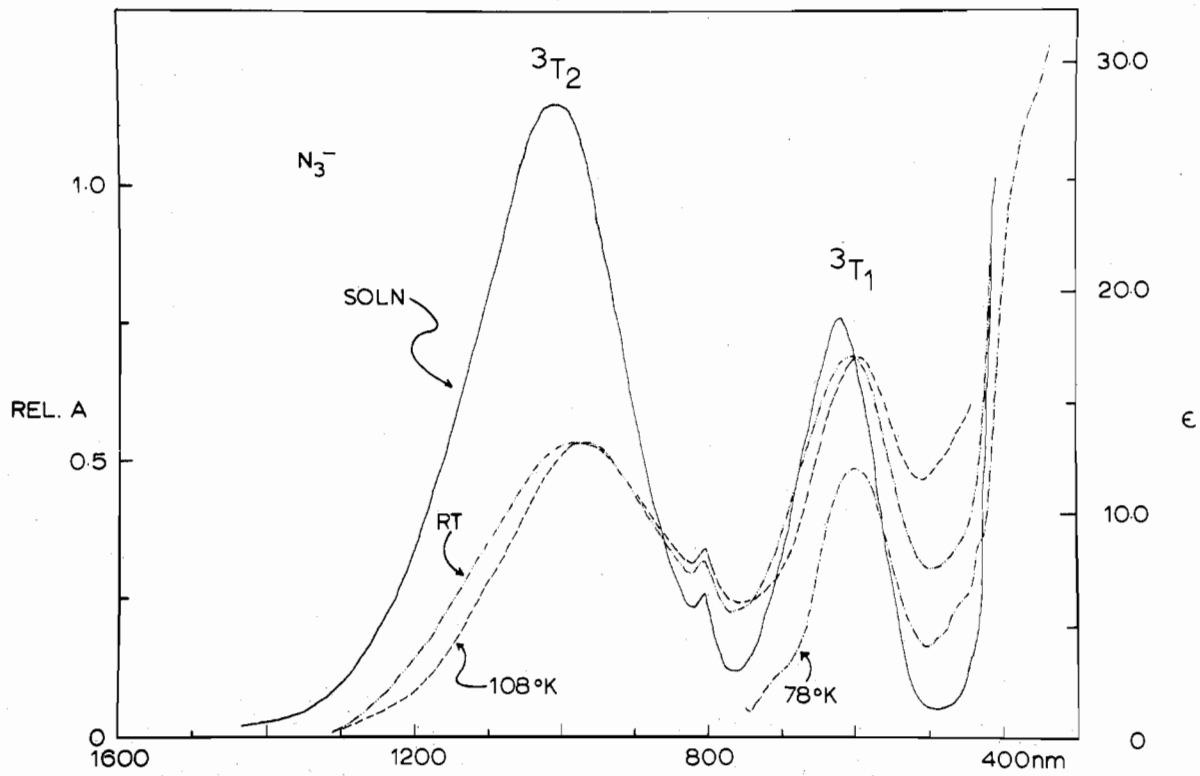

Figure 6. Electronic spectra of $[Ni(py)_4(N_3)_2]$. Refer to caption of Figure 5 and the labels of this figure.

clusion will also be important in the understanding of the MCD spectra of these compounds (*vide infra*). By a process of elimination we therefore conclude that the shoulders are of combined spin-orbit and vibronic origin, and our 4°K work in progress is anticipated to give us additional insight.

Another feature of interest is the decrease in integrated intensity with decreasing temperature of $^3T_{2g}$ and $^3T_{1g}$-$(t_2^5e^3)$, leading us to believe that transitions to these two excited states are vibronically allowed at least in part. However, the azide compound (Figure 6) showed the smallest temperature dependence of the three (NCO^-, NCS^-, N_3^-) on the basis of comparing ambient with 108°K spectra. With the aid of the 78°K spectrum we were also able to locate $^3T_{1g}(t_2^4e^4)$ as a prominent shoulder near 380 nm (Figure 6), and this was advantageously confirmed in the 44.0-kG MCD spectrum to be shown below.

Table IV. "Octahedral" State Energies of *trans*-$[Ni(py)_4L_2]$ in kK (nm)

L^-		$^3T_{2g}(F)$	$^1E_g(D)$	$^3T_{1g}(F)$	$^3T_{1g}(P)$
NCO^-	Ambient	10.13 (987)	13.04 (767)	16.67 (600)	26.88 (372)
	N_2(l)	10.36 (965)	13.07 (765)	17.24 (580)	27.17 (368)
				15.75 sh (635)	
NCS^-	Ambient	10.53 (950)	13.00 (769)	17.24 (580)	27.40 (365)
	N_2(l)	10.75 (930)	13.16 (760)	17.54 (570)	
$NCSe^-$	Ambient	10.59 (944)	13.16 (760)	17.54 (570)	
N_3^- [a]	Ambient	9.90 (1010)	12.42 (805)	16.26 (615)	
	N_2(l)	10.26 (975)	12.47 (802)	16.80 (595)	
				13.89 sh (720)	

[a] $^1\Gamma$ bands at 20.62, 21.74, 23.26 kK (or 485, 460, 430 nm).

A third noteworthy structural detail was the uncovering of three low-intensity bands between 400 and 500 nm of the azide spectrum (Figure 6). We assign them to $^1A_{1g}(G)$, $^1T_{2g}(D)$, and $^1T_{1g}(G)$ in order of increasing energy, on the basis of our detailed computational result of $[Ni(NH_3)_6]^{2+}$ described above. The 79°K spectrum of $[Ni(py)_4(NCO)_2]$ also made possible the observation of $^1\Gamma$ structure in the same wavelength region, but individual bands are less distinct.

A fourth point is that bands $^3T_{2g}$, $^3T_{1g}(F)$, and $^3T_{1g}(P)$ are twice as large for the N_3^- compound as for the analogous NCO^-, NCS^-, and NCS^- complexes. The most probable cause for this is the absence of centricity in the azide complex (also see MCD below). Partial support for this suggestion is that the radial penetration of the central nitrogen of N_3^- into Ni(II) is still substantial even though it is not formally bound to nickel (Figure 7). A cis configuration cannot entirely by discounted, however.

Finally, the rather intense first and second overtones of pyridine (ν(C-H)), which were so obvious in the halogen complexes described above, are notably absent in the pseudohalogen compounds. This is accidental in part; *i.e.*, there was no need to extend our measurements into the first overtone region near 1680 nm due to the higher energy location of $^3T_{2g}(t_2^5e^3)$. However, our original electronic spectra actually do show small shoulders near 1120 nm; *e.g.*, there is clearly a sharp shoulder in the spectrum of $[Ni(py)_4(NCS)_2]$.

4. Magnetic Circular Dichroism of $[Ni(py)_6]^{2+}$ and $[Ni(py)_4L_2]$, Where $L^- = NCO^-, NCS^-, NCSe^-$, and N_3^-. The most obvious factor these compounds have in common when one discusses their d-d transitions is the $Ni^{II}N_6$ chromophore, which of course applies also to $[Ni(NH_3)_6]^{2+}$. For this reason the salient features of the MCD spectrum[3,36] of the similar hexaammine as reported by Harding, Mason, Robbins, and Thomson[3] (HMRT) will be reviewed first. They reported MCD data for states $^1E_g(G)$, part of $^3T_{2g}(F)$, $^3T_{1g}(P)$, and $^3T_{1g}(F)$, but emphasis was placed on the last two states, especially $^3T_{1g}(F)$, because the experimental and interpretive information is most interesting and complete. First, the MCD activity of the $^3T_{1g}$ state of the hexaammine resides in the spin-orbit components Γ_1, Γ_3, Γ_4, and Γ_5 of this t_{1u} ^{v}-allowed vibronic band. Second, in view of quenched or very small A terms relative to $(B + C/kT)$ terms, the sum of the rotational strengths of $(B + C/kT)$ terms of these four spin-orbit components should vanish within first-order spin-orbit coupling theory.[37] In fact, the magnitude of the integrated residual activity (R) divided by the dipole strength (D_0) will be a measure of the extent of interterm second-order spin-orbit coupling. Third, it was found by HMRT that the second-order spin-orbit coupling between $^3A_{2g}(t_2^6e^2)$ and the first spin-allowed state, $^3T_{2g}(t_2^5e^3)$, can reasonably account for the observed MCD intensities in $^3T_{1g}(t_2^5e^3)$ and $^3T_{1g}(t_2^4e^4)$ by means of $(B + C/kT)$ terms of the spin-orbit components. Thus the large negative residual MCD activity of these two states can be understood; *e.g.*, the C term is primarily a consequence of $^3T_{2g}$ *orbital* angular momentum in $^3A_{2g}'$ and not due to the *spin* angular momentum of $^3A_{2g}$, where $\psi(^3A_{2g}') = c\phi(^3A_{2g}) + d\phi(^3T_{2g})$, as a consequence of $\langle ^3A_{2g}|L|^3T_{2g}\rangle \in A_{1g}$, and $\phi(^3A_{2g})$ and $\phi(^3T_{2g})$ are the first-order functions of the second-order Zeeman interaction.

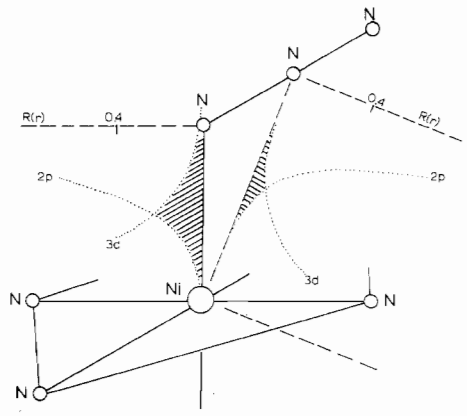

Figure 7. Amplitudes of Ni(3d) and N(2p) *normalized* radial function, $R(r)$, as a function of internuclear distances in the $Ni(N_3)$ moiety.

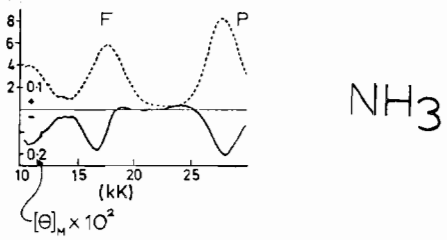

Figure 8. MCD spectrum of $[Ni(NH_3)_6]^{2+}$.[3]

Figure 8[3] shows a composite of MCD and electronic absorption spectra of $[Ni(NH_3)_6]^{2+}$ in aqueous solution as recorded by HMRT, with $^3T_1(F) \sim 17.5$ kK (570 nm) and $^3T_1(P) \sim 28$ kK (360 nm). For $^3T_{1g}(F)$ there is a small positive band near 18.5 kK (540 nm) and a much larger negative band which minimizes near 16.5 kK (606 nm), *i.e.*, a large, positive residual $(B + C/kT)$ term giving rise to the ratio $(B + C/kT)/D = +0.72 \times 10^{-3}$ β/cm^{-1}, and the theoretically computed value had the comparatively reasonable sign and magnitude of $+0.83 \times 10^{-3}$ β/cm^{-1}. Similarly, the positive residual $(B + C/kT)$ term is obvious from that figure for the $^3A_{2g} \rightarrow {}^3T_{1g}(P)$ manifold near 27.5 kK (364 nm), the transition having large negative rotation. However, we add that our 80°K electronic absorption data and calculations (*vide supra*) make it possible to conclude definitely that the small positive band of $[Ni(NH_3)_6]^{2+}$ near

(36) P. N. Schatz, A. J. McCaffery, W. Suetaka, G. N. Henning, A. B. Ritchie, and P. J. Stephens, *J. Chem. Phys.*, **45**, 722 (1966).
(37) R. G. Denning and J. A. Spencer, *Symp. Faraday Soc.*, **3**, 84 (1969).

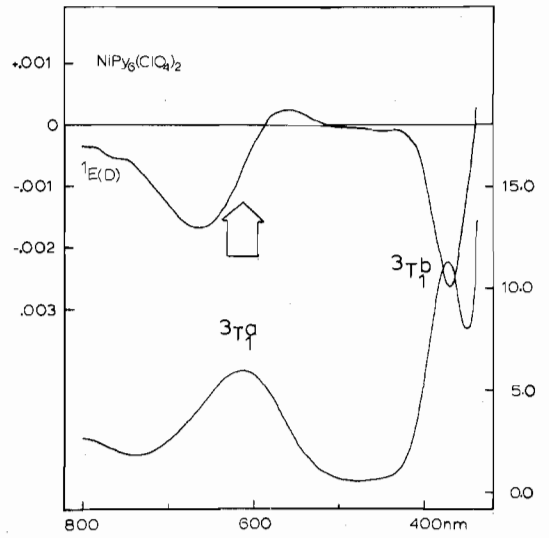

Figure 9. The 44,400-G MCD spectrum of $[Ni(py)_6](ClO_4)_2$. $[\theta]_M$ is the molar ellipticity per gauss (deg cm^2 dmol^{-1} G^{-1}).

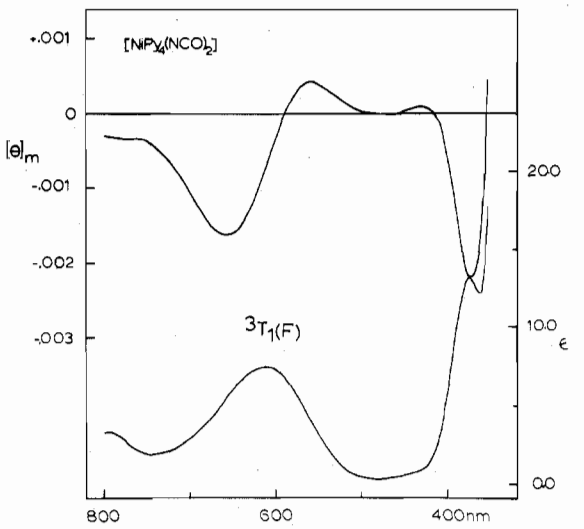

Figure 10. MCD spectrum of $[Ni(py)_4(NCO)_2]$.

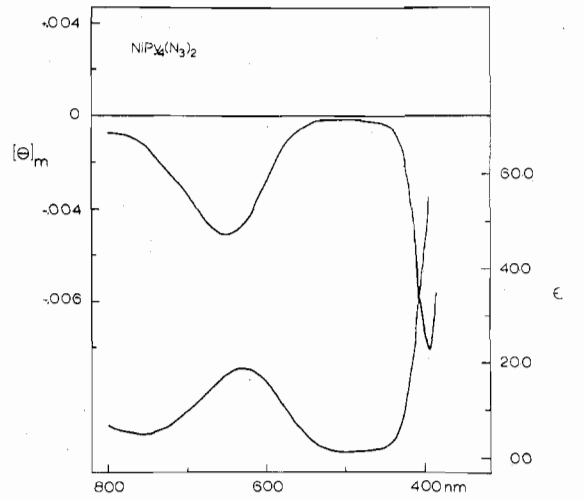

Figure 11. MCD spectrum of $[Ni(py)_4(N_3)_2]$.

24.5 kK must contain the MCD activity of $^1T_{2g}(D; t_2^4e^4)$, and perhaps in its red tail even $^1A_{1g}(G; t_2^6e^2)$. The sign of the calculated[3] activity of $^1T_{2g}(D)$ also agrees with the positive ellipticity observed. Further, the large negative MCD band near 27.5 kK (364 nm) must also host the $^3A_{2g} \rightarrow {}^1T_{1g}(G; t_2^5e^3)$ activity, since use of the "exact" spin-orbit crystal field matrices predict it (Γ_5) to be very close to the ($\Gamma_3, \Gamma_5, \Gamma_4, \Gamma_1$) manifold of $^3T_1(P)$ (see Figure 1 and Table I). Whereas the $^1T_{1g}(G)$ activity relative to $^3T_{1g}(P)$ is expected to be very small, the $^1T_{2g}(D)$ activity is expected to be that of the observed 24.5-kK (480-nm) band. The MCD results for $[Ni(py)_2L_2]^0$ (L = py, NCO^-, NCS^-, $NCSe^-$, N_3^-) will be discussed with the above conclusions in mind and will be compared to them.

We show our solution MCD spectra in Figures 9-11 (L = py, NCO^-, N_3^-), each having been measured at 44,400 G. The MCD spectra of L = NCS^- and $NCSe^-$ are nearly superimposable on that of L = NCO^- (Figure 10). Data for all compounds can be found in Table V-VII. The solution concentrations were kept at optical density of *ca.* 2.0 or less. In view of our available instrumental range, the MCD data cover the $^1E_g(D)$, $^3T_{1g}(F)$, $^1T_{2g}(D)$, and $^3T_{1g}(P)$ states. The spin singlets $^1A_{1g}(G)$ and $^1T_{1g}(G)$ are predicted between $^3T_{1g}(F)$ and $^3T_{1g}(P)$, but no distinct MCD activity identifies them since the expectedly weak $^1T_{1g}(G)$ is nearly degenerate with the intense $^3T_{1g}(P)$, and $^1A_{1g}(G)$ has apparently very little activity. We therefore expect to see two intense and two weak bands in the range 800-350 nm. $^3T_{1g}(F)$ near 600 nm will be of primary interest.

Figure 9 shows the MCD spectrum of $[Ni(py)_6]^{2+}$ and how the electronic absorption and MCD spectra align. The ~780-nm MCD band is $^1E_g(D)$, but the spectrum does not clarify the location of $^1T_{2g}(D)$, expected near ~450 nm. It is interesting to point out the close similarity of this spectrum with that of $[Ni(NH_3)_6]^{2+}$; *viz.*, $^3T_{1g}(F)$ near 600 nm has a small positive component but a large negative residual ($B + C/kT$) term; the MCD of $^3T_{1g}(P)$ minimizes at the electronic band maximum near 480 nm; and $[\theta]_{max}[^3T_1(P)] > [\theta]_{max}[^3T_1(F)]$. However, while transitions to $^3T_{1g}(F)$ of $[Ni(NH_3)_6]^{2+}$ and $[Ni(py)_6]^{2+}$ have about the same dipole strengths, the rotational strength and residual ($B + C/kT$)/D term, R/D_0, of $[Ni(py)_6]^{2+}$ is significantly smaller. For example, we obtain $R/D_0 \approx 0.59 \times 10^{-3}$ β/cm^{-1} (Table V) from gaussian analysis and *ca.* 0.54×10^{-3} β/cm^{-1} (Table VII) from the method of moments for $[Ni(py)_6]^{2+}$, whereas for $[Ni(NH_3)_6]^{2+}$ this residual parameter has the larger value 0.72×10^{-3} β/cm^{-1}.[3] These *relative* values are contrary to what one expects solely on the basis of the $^3A_{2g}$–$^3T_{2g}(F)$ mixing, since the energy separation of these two states is 10.2 kK for $[Ni(py)_6]^{2+}$ but 10.75 kK for $[Ni(NH_3)_6]^{2+}$, or $[Ni(py)_6]^{2+}$ should have a larger residual C term. Furthermore, other $^3\Gamma$ d-d states are closer to $^3T_{1g}(F)$ in $[Ni(py)_6]^{2+}$ than in $[Ni(NH_3)_6]^{2+}$ (Table IV) which would result in larger B terms for the hexapyridine complex. We attribute the smaller experimental R/D_0 value of $[Ni(py)_6]^{2+}$ to a lower

Table V. Gaussian Fit of $^3T_{1g}(F)$: Method A[a]

	ν^0, nm (kK)	Δ_0, kK	A^b	$10^5 \times B^b$	A/D_0	$10^3 \times B/D_0$	$10^4\sigma$
$Ni(py)_4(N_3)_2$	615 (16.26)	1.80	0.010	3.00	0.28	0.85	5.97
$[Ni(py)_6]^{2+}$	605 (16.53)	1.80	0.010	0.78	0.75	0.59	2.93
$Ni(py)_4(NCSe)_2$	570 (17.54)	1.80	0.028	1.25	1.31	0.59	5.86
$Ni(py)_4(NCO)_2$	600 (16.67)	1.80	0.0105	0.65	0.70	0.43	3.71
$Ni(py)_4(NCS)_2$	580 (17.24)	1.80	0.0135	0.80	0.61	0.36	2.42
$[Ni(NH_3)_6]^{2+}$						0.72[c]	

[a] ν^0 is the electronic absorption band maximum. [b] Units: A, $D^2\beta$; B, $D^2\beta$/cm^{-1}; D_0, D^2. [c] Reference 3.

Table VI. Gaussian Fit of $^3T_{1g}(F)$: Method B

	ν^0,[a] nm (kK)	Shifted[b] ν^0_0, nm (kK)	Δ_0, kK	A[c]	10^5B	A/D_0[c]	$10^3B/D_0$	$10^4\sigma$
$Ni(py)_4(N_3)_2$	615 (16.26)	627.5 (15.95)	1.80	0.010	3.00	0.28	0.85	1.72
$[Ni(py)_6]^{2+}$	605 (16.53)	619 (16.16)	1.80	0.010	0.75	0.75	0.56	0.31
$Ni(py)_4(NCSe)_2$	510 (17.54)	580 (17.24)	1.70	0.025	1.05	1.17	0.49	2.09
$Ni(py)_4(NCO)_2$	600 (16.67)	620 (16.13)	1.80	0.011	0.65	0.73	0.43	0.69
$Ni(py)_4(NCS)_2$	580 (17.24)	588 (17.01)	1.75	0.013	0.80	0.59	0.36	1.21
$[Ni(NH_3)_6]^{2+}$							0.72[d]	

[a] Electronic absorption maximum. [b] Value of ν^0 used in the calculation. [c] See footnote *b* of Table V. Dipole strength obtained from moment analysis. The A term width parameter is $\Gamma = \sqrt{2}\Delta_0 = 2550$ cm^{-1}. [d] Reference 3.

Table VII. Residual MCD Parameter $(B_{II} + C_{II}/kT)$[a] of $^3A_{2g} \rightarrow {}^3T_{1g}(F)$ by Method of Moments[b]

	$10^5(B_{II} + C_{II}/kT)$	$10^3(B_{II} + C_{II}/kT)/D_0$	Ref
$Ni(py)_4(N_3)_2$	3.0	0.86	*b*
$[Ni(NH_3)_6]^{2+}$		0.72	*c*
$[Ni(py)_6]^{2+}$	0.71	0.54	*b*
$Ni(py)_4(NCSe)_2$	0.92	0.43	*b*
$Ni(py)_4(NCO)_2$	0.57	0.38	*b*
$Ni(py)_4(NCS)_2$	0.68	0.31	*b*

[a] Units are β D^2/cm^{-1}. [b] Moment analysis for D_0 and $(B_{II} + C_{II}/kT)$. [c] Approximate moment analysis by authors of ref 3 gave the indicated value of $(B_{II} + C_{II}/kT)/D_0$.

electronic symmetry than is present in $[Ni(NH_3)_6]^{2+}$ which in turn would have a quenching effect on the C terms in $^3A_{2g} \rightarrow {}^3T_{1g}(F)$.

A similar situation prevails for $[Ni(py)_4(NCO)_2]$ (Figure 10), where $^3T_{1g}(F)$ has the somewhat larger zeroth-moment dipole strength, $D_0 = 1.51 \times 10^{-2}$ D^2, compared to $[Ni(py)_6]^{2+}$ (1.33×10^{-2} D^2) but the MCD patterns of the two compounds are very alike (Figures 9 and 10) for $^3T_{1g}(F)$ and $^3T_{1g}(P)$ near 600 and 400 nm, respectively. The dipole strength difference leads to the smaller value of $(B + C/kT)/D_0$ of $^3T_{1g}(F)$ for $[Ni(py)_4(NCO)_2]$ (0.38×10^{-3} β/cm^{-1}) and $[Ni(py)_6]^{2+}$ (0.54×10^{-3} β/cm^{-1}) (Table VII). The results from the gaussian analysis (Table VI) are similar, 0.43×10^{-3} and 0.56×10^{-3} β/cm^{-1} for the NCO^- and hexapyridine complexes. It can also be noted that the positive $^1T_{2g}(D)$ band of $[Ni(py)_4(NCO)_2]$ near 430 nm is very well resolved in the ambient MCD spectrum, as also in the 79°K electronic spectrum, but not in the ambient electronic spectrum. The activity of $^3T_{1g}(P)$ is such that the rotational minimum coincides with the electronic absorption band maximum of *ca.* 380 nm.

As one takes a careful look at the NCS^- and $NCSe^-$ compounds, it becomes apparent that the electric dipole strengths are larger than the ones of the NCO^- complex (2.2×10^{-2}, 2.1×10^{-2}, and 1.51×10^{-2} D^2 for NCS^-, $NCSe^-$, and NCO^-). It is reasonable to assume that the closer proximity of the very intense internal NCX^- (X = S, Se) transitions can in large part be a cause of this. This also affects the net $^3T_{1g}(F)$ rotational strength of the NCS^- compound to some extent, *i.e.*, increasing it, and to the largest degree in $[Ni(py)_4(NCSe)_2]$. For example, in the latter compound the peak-to-trough value of $^3T_{1g}(F)$ nearly doubles and the residual $(B + C/kT)$ term (Table VII) is much larger than in $[Ni(py)_6]^{2+}$ and $[Ni(py)_4(NCX)_2]$ (X = O, S). We tentatively suggest that this dramatic MCD intensity increase is the result of additional second-order spin-orbit coupling of $^3T_{1g}(F)$ components with those of $NCSe^-$ "ligand transitions." It was also found that $^1T_{2g}(D)$ has positive rotational strength as predicted theoretically for the very analogous $[Ni(NH_3)_6]^{2+}$.[3]

The MCD dispersion through $^3T_{1g}(F)$ of $[Ni(py)_4(N_3)_2]$ is dramatically different from the other MCD spectra discussed thus far; *viz.* the high-energy positive rotational structure (Γ_3, Γ_5) of $^3T_{1g}(F)$ vanished (Figure 11). One contributor to this difference may be the lower microsymmetry about Ni(II), as also reflected by the significantly larger electric dipole strength (3.5×10^{-2} D^2) and the feasibly associated annihilation of C terms. The MCD spectrum had the advantage of cleanly uncovering the position of $^3T_{1g}(P)$ near 400 nm, which was only an ill-defined shoulder in the 78°K electronic absorption spectrum. It is of additional interest now to note that the $^3T_{1g}(P)$ and $^3T_{1g}(F)$ transition energies are less for the N_3^- complex than the other pseudohalogen (NCO^-, NCS^-, $NCSe^-$) compounds (Table IV). Perhaps the larger spatial requirement of the bent Ni–NNN group results in the Ni–N distance being larger than the ones in Ni–NCX (X = O, S, Se).

5. Moment Analysis of the $^3A_{2g} \rightarrow {}^3T_{1g}(F)$ Transition. The recent paper by Stephens[38] reiterated the desirability of using moment analysis, introduced by Henry, Schnatterly, and Slichter,[39] for purposes of deriving accurate Faraday parameters from experimental spectra. Thus, the nth moments[40] of electronic absorption and MCD bands, $\langle\epsilon\rangle_n$ and $\langle\theta\rangle_n$, are given by

$$\langle\epsilon\rangle_n = \int(\epsilon/\nu)(\nu - \nu^0)^n \, d\nu$$

$$\langle\theta\rangle_n = \int(\theta_M/\nu)(\nu - \nu^0)^n \, d\nu$$

where $\langle\epsilon\rangle_1 = 0$ defines ν^0, and the other symbols have their usual meanings. Accurate dipole strengths, D_0, and $(B + C/kT)$ parameters, for example, are directly related to the zeroth moments $\langle\epsilon\rangle_0$ and $\langle\theta\rangle_0$. We derived these moments for $[Ni(py)_6]^{2+}$ and $[Ni(py)_4L_2]$ ($L^- = NCO^-$, NCS^-, $NCSe^-$, N_3^-) for the transition $^3A_{2g} \rightarrow {}^3T_{1g}(F)$ and the Faraday parameters were calculated as entered in Table VII. These parameters are valuable since the magnitudes reflect the extent of second-order interstate spin-orbit coupling of $^3A_{2g}$ with $^3T_{2g}(F)$[3,37] and of $^3T_{1g}(F)$ with other appropriate excited states. Thus, the results of Denning and Spencer[37] can be used here to infer that in the absence of second-order spin-orbit coupling the net C term over the $^3T_{1g}(F)$ spin-orbit components should vanish, as should the sum of B terms. However, mixing $^3T_{2g}(F)$ with $^3A_{2g}$, for example, will result in nonvanishing B and C terms,[3] B_{II} and C_{II}, where $B_{II} \propto 1/$

(38) P. J. Stephens, *Chem. Phys. Lett.*, 2, 241 (1968).
(39) C. H. Henry, S. E. Schnatterly, and C. P. Slichter in "Physics of Color Centers," W. B. Fowler, Ed., Academic Press, New York, N. Y., 1968, p 351.
(40) P. J. Stephens, R. L. Mowery, and P. N. Schatz, *J. Chem. Phys.*, 55, 224 (1971).

($^3T_{2g}$-$^3A_{2g}$) and $C_{II} \propto \gamma$, with γ the mixing coefficient in the expression for the modified ground state, $|A_{2g}> = |^3A_{2g}> + \gamma|^3T_{2g}>$. Thus, for octahedral nickel(II) compounds in which only $^3A_{2g}$-$^3T_{2g}$ mixing is important one would expect to observe the proportionality

$$[B_{II} + C_{II}/kT] \propto \left[\frac{1}{^3T_{2g}-^3A_{2g}} + \frac{\gamma}{kT}\right]$$

i.e. the absolute value of the net term $[B_{II} + C_{II}/kT]$ should increase with decreasing separation ($^3T_{2g}$-$^3A_{2g}$) and with increasing mixing coefficient. But since $\gamma = 2\zeta/10Dq$, one can write[3]

$$[B_{II} + C_{II}/kT] \propto \left[\frac{1}{^3T_{2g}-^3A_{2g}} + \frac{2\zeta}{10Dq(kT)}\right]$$

In summary, the residual Faraday ($B + C/kT$) parameter ought to increase with decreasing ($^3T_{2g}$-$^3A_{2g}$) and ($^3T_{1g}$-$^3A_{2g}$) separations. We find by the method of moments that ($B + C/kT$) varies as $[Ni(NH_3)_6]^{2+} < [Ni(py)_4(NCO)_2] < [Ni(py)_4(NCS)_2] < [Ni(py)_6]^{2+} < [Ni(py)_4(NCSe)_2] < [Ni(py)_4(N_3)_2]$, which does not parallel the $^3A_{2g}$-$^3T_{2g}$ energy separation. If one takes into account the variation of dipole strength by evaluating the ratios $(B + C/kT)/D_0$, these latter values then vary as $[Ni(py)_4(NCS)_2] < [Ni(py)_4(NCO)_2] < [Ni(py)_4(NCSe)_2] < [Ni(py)_6]^{2+} < [Ni(NH_3)_6]^{2+} < [Ni(py)_4(N_3)_2]$. This variation does also not follow the trend of $^3A_{2g}$-$^3T_{2g}$ separations (Table IV). This leads us to conclude that simple $^3A_{2g}$-$^3T_{2g}$ mixing is perhaps insufficient to account for minor variations. The overall nature of the model is obviously correct. Thus, the interaction between $^3T_{1g}(F)$ and other appropriate excited states must play an important role in destroying the order of the *expected* sequence based on only the $^3A_{2g}$-$^3T_{2g}$ mixing, or $[Ni(NH_3)_6]^{2+} < [Ni(py)_6]^{2+} \sim [Ni(py)_4(NCO)_2] < [Ni(py)_4(NCS)_2] \sim [Ni(py)_4(NCSe)_2]$.

The compounds most similar in this seven-membered series are $[Ni(py)_4(NCO)_2]$ and $[Ni(py)_4(NCS)_2]$ from the point of view of nuclear geometry and types of electronic transitions near $^3A_{2g} \rightarrow {}^3T_{1g}(F)$. For these compounds at least the relative magnitudes of the residual ratio $(B + C/kT)/D_0$ are directionally correct (0.31×10^{-3} and 0.38×10^{-3} β/cm^{-1} for NCS^- and NCO^-) for $^3A_{2g}$-$^3T_{2g}(F)$ mixing, and also the $^3T_{1g}(F)$ states are in the order $NCS^- > NCO^-$ (Table IV).

Now we compare residual parameters for $^3T_{1g}(F)$ as derived from gaussian analysis (Table VI) with those from moment analysis (Table VII). For either the $[Ni(py)_4(N_3)_2]$ or $[Ni(py)_6]^{2+}$ complex the two methods give the same parameter values. The gaussian values of the other three pyridine complexes are about 10% larger than for the moment values. Finally, it is pointed out that in the gaussian fitting procedure of $^3T_{1g}(F)$, it was necessary to use ν^0 values slightly different from the values of ν_{max} of electronic absorption bands in order to obtain a reasonably good one-band fit. The shift is small and always to lower energy for best results. Standard deviations may be compared in Tables V and VI, and the optimized values of ν^0 of Table VI are obviously superior. For example, with the $[Ni(py)_6]^{2+}$ spectrum the adjusted ν^0 (from 16.53 to 16.16 kK) results in a good fit with standard deviation 0.31×10^{-4}, whereas one obtains a very poor fit if the apparent solution electronic absorption band maximum (16.53 kK) is chosen for ν^0.

6. MCD of *trans*-$[Ni(py)_4X_2]$, Where $X^- = Cl^-$, Br^-, and I^-. The MCD spectra of the chloro and bromo compounds are shown respectively in Figures 12 and 13. There is an astounding similarity of $^3T_{1g}(F)$ dispersions among $[Ni(py)_4Cl_2]$, $[Ni(py)_6]^{2+}$, and all the pseudohalogen complexes but

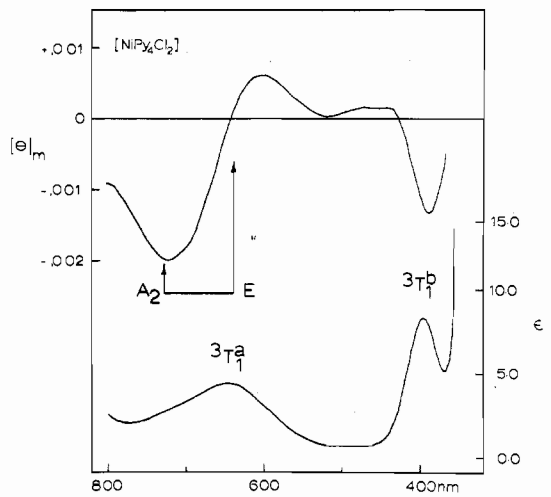

Figure 12. The 44,400-G MCD spectrum of $[Ni(py)_4Cl_2]$.

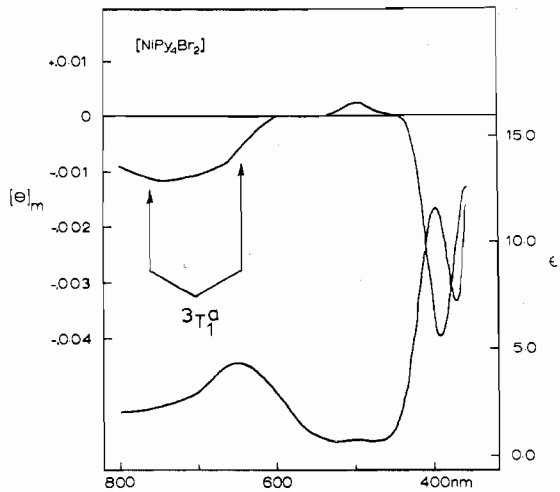

Figure 13. The 44,600-G MCD spectrum of $[Ni(py)_4Br_2]$.

the azide one (compare Figure 12 with Figure 11). For example, the peak-to-trough molar ellipticity values, $[\theta(P)]$, of $[Ni(py)_4Cl_2]$ and $[Ni(py)_2(NCO)_2]$ are nearly equal, but the ratio $[\theta(P)]/D$ of the dichloro molecule is about 2 times larger. However, this ratio $[\theta(P)]/D$ of $[Ni(py)_4Cl_2]$ is so similar to the other $Ni^{II}N_6$ molecules discussed above, that we consider the MCD intensity of this $^3T_{1g}(F)$ dispersion can be understood in a manner of the O_h chromophore $Ni^{II}N_6$ in spite of an expected enhancement of intensity due to the presence of an internal heavy atom (Cl). It is very interesting that $^3E_g(T_{1g})$ near 630 nm displays the positive lobe of an *apparent A* term with an estimated Faraday parameter ratio $A/D \approx 0.18\ \beta$, but the interpretive work discussed above mitigates against it being a genuine A term. The positive MCD activity of $^1\Gamma$ states, which were also located in the liquid N_2 electronic spectrum, show up between 450 and 500 nm with the usual positive sign. The activity of "$^3T_{1g}$(P)" of $[Ni(py)_4Cl_2]$ differs from the analogous activities of NiN_6 compounds discussed already only in that its $|\theta_{max}|$ value is only about 50% the magnitude of the "$^3T_{1g}(F)$" peak-to-trough magnitude, $[\theta(P)]$, whereas in the NiN_6 compounds the magnitudes of $[\theta(P), {}^3T_{1g}(F)]$ are usually equal to or smaller than $|[\theta_{max}, {}^3T_{1g}(P)]|$.

The MCD spectra of $[Ni(py)_4Br_2]$ (Figure 13) and of $[Ni(py)_4I_2]$ in the region of $^3T_{1g}(F)$ differ from the same region for $[Ni(py)_4Cl_2]$; *viz.*, the chloro complex still has the now familiar positive lobe on the blue side of the band, whereas this positive lobe vanishes in the bromo and iodo

compounds. However, the residual ratios $(B + C/kT)/D_0$ of the three compounds are of about the same magnitude. The rather large electric dipole strength and large residual $(B + C/kT)$ term of the iodo compound compared to the bromo compound may in part originate from a larger internal heavy-atom effect, I > Br.

7. **Preliminary Crystal Structure Parameters of $[Ni(py)_4I_2]$.** Partly because the $^3T_{1g}(F)$ residual MCD activity of the three halogen compounds is oddly $I^- > Cl^- > Br^-$, the single-crystal X-ray diffraction study of $[Ni(py)_4I_2]$ was undertaken in this laboratory.[41] Several structural parameters of the dichloro and dibromo analogs had already been obtained a number of years ago.[42] Our crystal of $[Ni(py)_4I_2]$ was found to be orthorhombic, of space group D_{2h}^{14} (No. 60), $d = 1.878$ g/cm^3 (floatation) and $Z = 4$. With $R = 0.064$ the unit cell dimensions were found to be 9.678, 16.076, and 14.004 Å for *a*, *b*, and *c*. The average Ni-N distance is 2.11 Å and Ni-I is 2.88 Å. It is at the moment impossible to determine if the *Dq* parameter of py should vary as reflected in Table III (I > Cl > Br), since from the previously reported study[42] all one knows is that the Ni-N(py) interatomic distance of $[Ni(py)_4Br_2]$ falls in the range 2.0-2.2 Å, and the Ni-N(py) value of $[Ni(py)_4Cl_2]$ was not given in the report.[42] There is the additional difficulty that the chloro and bromo crystals lose pyridine rapidly. The full structural report of $[Ni(py)_4I_2]$ will be the subject of our next article.[41]

(41) D. J. Hamm, J. Bordner, and A. F. Schreiner, *Inorg. Chim. Acta*, in press.
(42) M. A. Porai-Kashits, A. S. A. Antzishkina, L. M. Dichareva, and E. K. Jukhnov, *Acta Crystallogr.*, **10**, 784 (1957).

Registry No. $[Ni(py)_4(N_3)_2]$, 40354-94-7; $Ni(NH_3)_6Cl_2$, 10534-88-0; $Ni(NH_3)_6(ClO_4)_2$, 14322-50-0; $[Ni(C_5H_5N)_4Cl_2]$, 14077-26-0; $[Ni(C_5H_5N)_4Br_2]$, 14129-05-6; $[Ni(C_5H_5N)_4I_2]$, 14077-31-7; $[Ni(C_5H_5N)_4(NCO)_2]$, 28131-44-4; $[Ni(C_5H_5N)_4(NCS)_2]$, 30868-61-2; $[Ni(C_5H_5N)_4(NCSe)_2]$, 15277-22-2; $[Ni(py)_6](ClO_4)_2$, 18346-94-6.

Acknowledgments. Computer calculations were carried out on the IBM 370/165 of the Triangle Universities Computation Center (TUCC). We thank the School of Physical and Mathematical Sciences of this University for funding the liquid helium. We also acknowledge our discussion with Professor R. S. Drago regarding the chemical nature of $[Ni(py)_6]^{2+}$.

Contribution from the Department of Chemistry, Emory University, Atlanta, Georgia 30322

Mercuric Ion Induced Hydrolysis of *trans*-Dibromodinitroethylenediamineplatinum(IV)

W. LAWRENCE DICKINSON and RONALD C. JOHNSON*

Received January 15, 1973

The hydrolyses of *trans*-$Pt(NH_3)_4Cl_2^{2+}$, *trans*-$Pt(NH_3)_4Br_2^{2+}$, and *trans*-$Pt(en)(NO_2)_2Br_2$ do not occur in acidic aqueous solution. The former two compounds also do not hydrolyze to any extent in an acidic 0.010 *M* mercuric nitrate solution. The latter compound does react completely to form $Pt(en)(NO_2)_2BrOH$. The reaction rate is first order with respect to the platinum(IV) complex, mercuric ion, and the catalyst $Pt(en)(NO_2)_2$ and at 25.0° has a rate constant of $1.7 \times 10^5\ M^{-2}$ sec^{-1}. The activation parameters are $\Delta H^* = 2.4$ kcal/mol and $\Delta S^* = -26.5$ cal/mol deg. An activated complex in which two single bromide bridges link the three metal ions is proposed.

Introduction

Little research has been published dealing with the mechanisms of hydrolysis reactions of platinum(IV) complexes in neutral or acidic solution. The available results deal with the anionic complexes $PtCl_6^{2-}$,[1] $PtBr_6^{2-}$,[2] PtI_6^{2-},[3] and $Pt(CN)_4Br_2^{2-}$.[4] The hydrolyses of the hexahalides lead ultimately to the loss of several halide ions. The rates of the reactions of the chloro and bromo complexes are quite sensitive to light. Dissociative processes and mechanisms involving redox have been proposed for both thermal and photochemical processes.

We are not aware of hydrolysis studies of neutral or acidic solutions of uncharged or cationic haloammineplatinum(IV) complexes. Aqueous solutions of complexes of this type can generally be kept for long periods without hydrolysis. This fact would account for the absence of hydrolysis studies. Data presented in this article indicate that two of these complexes are stable with respect to hydrolysis even in the presence of mercuric ion. Haloammineplatinum(IV) complexes do hydrolyze in basic solution and kinetic studies have been published.[5]

Mercuric ion has been used to accelerate the rate of hydrolysis of halo complexes of metal ions such as cobalt(III) and chromium(III).[6] The presence of mercuric ions can also shift an otherwise unfavorable hydrolysis equilibrium by complexing the halide ion as it is released.

Results and Discussion

The reactions of mercuric ion with several haloammineplatinum(IV) complexes were studied. Large changes were observed in the ultraviolet spectra of *trans*-$Pt(en)(NO_2)_2Br_2$ solutions when mercuric ions were added in the presence of $Pt(en)(NO_2)_2$.

Several types of evidence were collected to verify the identity of the platinum(IV) product. The suspected product, $Pt(en)(NO_2)_2BrOH$, was synthesized by the reaction of solutions of silver nitrate and $Pt(en)(NO_2)_2Br_2$. The fol-

(1) L. E. Cox, D. G. Peters, and E. L. Wehry, *J. Inorg. Nucl. Chem.*, **34**, 297 (1972).
(2) L. I. Elding and L. Gustafson, *Inorg. Chim. Acta*, **5**, 643 (1971).
(3) B. Corain and A. J. Poe, *J. Chem. Soc.*, 1633 (1967).
(4) C. E. Skinner and M. M. Jones, *J. Amer. Chem. Soc.*, **91**, 1984 (1969).
(5) R. C. Johnson, F. Basolo, and R. G. Pearson, *J. Inorg. Nucl. Chem.*, **24**, 59 (1962); A. A. Grinberg and A. A. Korableva, *Russ. J. Inorg. Chem.*, **11**, 409 (1966).
(6) J. N. Bronsted and R. Livingston, *J. Amer. Chem. Soc.*, **49**, 435 (1927); J. H. Espenson and J. P. Birk, *Inorg. Chem.*, **4**, 527 (1965).